Phase transition and thermodynamics of quantum XY model in two dimensions

H.-Q. Ding
Materials Simulation Center, Beckman Institute, California Institute of Technology, Pasadena, California 91125
(Received 15 July 1991)

The two-dimensional spin-$\frac{1}{2}$ XY model is investigated via an extensive quantum Monte Carlo simulation on square lattices as large as 128×128. The transverse susceptibility and correlation length show precise thermodynamic scaling behaviors of a phase transition of the Kosterlitz-Thouless type at $kT_c/J=0.353(3)$. The correlation functions near the transition point exhibit a universal scaling behavior. Various critical exponents are determined and our results demonstrate that the universality class of the two-dimensional quantum system with continuous symmetry is the same as its classical analog. The specific heat exhibits a finite peak around $kT/J=0.45$, decreases very rapidly near T_c, and falls off as T^2 near $T=0$, validating the spin-wave treatment. The ground-state energy is $-0.5543(1)J$ per spin.

I. INTRODUCTION

Recently, it was observed[1,2] that the resistivity in the superconducting single crystals drop to zero according to an exponential form typical of a Kosterlitz-Thouless[3] (KT) type singularity, at a temperature 0.2 K below the mean-field superconducting transition at $T_c^0=93.15$ K. This has brought renewed interest in the two-dimensional (2D) quantum XY model, which is expected to exhibit the KT-type singularity. Although the strongly correlated electrons in the CuO_2 planes do not bear much resemblance to the quantum spins, the latter can be mapped[4,5] into a quantum lattice fluid, which possesses the same symmetry as the original system. The O(2) symmetry here is the phase invariant of the system, $\psi_i\rightarrow\psi_i e^{i\alpha}$, for the bosonic field ψ_i. The XY model is thus a prototype for the study of the phase transition and condensation in 2D quantum systems with continuous symmetry.

Apart from the current interest, the 2D quantum model relates to a wide class of problems with similar symmetry properties, such as the superfluidity of ^{4}He in thin films. The connection also extends to cases where the symmetry is different. An example is the high-spin ferromagnetic (or antiferromagnetic) insulators with isotropic Heisenberg exchange interactions. If a large single-ion crystal field is present, the critical region is effectively dominated by the spin-$\frac{1}{2}$ XY interaction[5] because the matrix elements of the XY term are larger than the Ising term by a factor of $2(S+\frac{1}{2})^2$.

Finally, the existence and the nature of the phase transition in the 2D quantum XY model is a longstanding problem. The 2D classical version of the model (planar rotator model) undergoes a KT transition at $kT_c/J=0.898$,[6,7] characterized by an exponentially divergent correlation length and in-plane susceptibility. The transition, due to the unbinding of vortex-antivortex pairs, is weak; the specific heat has a finite peak above T_c. General universality arguments suggest that the same KT transition may occur in the quantum model. However, physics in two dimensions is characterized by large fluctuations, as demonstrated by the Mermin-Wagner theorem. Changing from the classical model to the quantum model, the additional quantum fluctuations (which are particularly strong in the spin-$\frac{1}{2}$ case) may alter the physics significantly. A possible consequence is that the already weak KT transition could be pushed down to zero temperature so that the topological order never occur. There had been studies on the quantum phase transition using the Landau-Ginzburg-Wilson functional approach, but, unfortunately, their results do not apply to 2D cases.[8]

The question of transition had been controversial. Analyzing a large-order high-temperature series, Betts and co-workers[5,9] suggested a conventional second-order transition at $kT_c/J=0.39$. A number of real-space renormalization-group (RSRG) analyses were applied[10] to this model. Unfortunately, their results are both inconclusive and contradictory. The main problem appears to be the difficulty in preserving the symmetry of the model when operators were constructed. As a result, RSRG has typically predicted a critical point for both the XY model and the Heisenberg model, a dilemma similar to the analysis of the high-temperature series.

Quantum Monte Carlo (QMC) simulations, using the Trotter-Suzuki transformation,[11] have long been employed to study this model,[12] along with other spin models. At the small-Trotter-number limit, DeRaedt, DeRaedt, Fivez, and Lagendijk[13] obtained an exact solution which suggests an Ising-like (second-order) transition at the Ising point $kT_c/J=[2\ln(1+\sqrt{2})]^{-1}=0.567$, with a divergent specific heat. They further supported their conclusion by QMC simulations. Loh, Scalapino, and Grant[14] carried out another simulation with the "world line" algorithm and found that the peak of specific heat remains finite. They argued that a KT phase transition occurs at $T_c=0.4$–0.5 by measuring the change of the "derivatives of helicity modulus." More recent QMC studies[15] to resolve this problem were either unclear or even more controversial.

These studies provide some qualitative features of a phase transition which appears to develop in the temperature range $kT/J=0.4$–0.56. Since the lattice systems studied are rather small, the singular behaviors of a phase transition were not identified. To unequivocally pin

down the existence of a transition and to classify the transition, we believe that the key question is how the correlation length and in-plane susceptibility behave as T_c is approached from above because their divergences constitute the most direct evidence of a phase transition. If we can clearly identify various scaling behaviors of the transition, we can further characterize the transition by the known types of transitions. Unfortunately, these long-range quantities are much more difficult to measure and large lattices are required in order to avoid finite-size effects. In previous works these studies are lacking.

Motivated from these considerations, we have carried out extensive simulations on much bigger lattices (as large as 128×128) with much better statistics. This was possible because of the algorithmic advances[16] and of the extensive use of the Caltech-JPL MarkIIIfp parallel computer,[17] which, in this case, is more powerful than the conventional vector computers such as a Cray XMP supercomputer.[18]

We are able to measure accurately both the spin-correlation functions with correlation lengths from $0.56a$ to $43.4a$, and the in-plane susceptibility, both of which are found to diverge at transition point, $kT_c/J=0.353$, according to the Kosterlitz-Thouless scaling form. The correlation functions measured are found to obey the universal scaling with the critical exponent $\eta=0.276\pm0.014$ (quite consistent with $\eta=\frac{1}{4}$ expected for the classical model). This is further confirmed by several finite-size scalings at the transition point. Therefore, the universality class of the quantum transition is the same as the classical transition. We measured various thermodynamical quantities. At high temperatures, $T>0.8J$, our results agree very well with the high-temperature series expansions.[9] Near $T=0$, we found a T^3 behavior for the energy density and a T^2 power law for the specific heat. This result indicates a linear excitation spectrum, $E(k)\sim k$, at low temperature and thus validates the spin-wave analysis of this model.[19] The specific heat increase very rapidly around T_c and exhibits a finite peak at $T=0.45J$. We also extracted the ground-state energy, which is in excellent agreement with both spin-wave results and the finite cluster calculations.[20]

The rest of the paper is organized as the following. In Sec. II, the quantum Monte Carlo algorithm and simulation details are explained. Section III contains the main points of this work. Various scaling behaviors of the system near T_c are discussed. Convincing numerical evidence for the existence of the KT transition are presented. In Sec. IV, thermodynamic quantities both at the high-temperature region and at the low-temperature region, especially the behavior near $T=0$, are discussed. Concluding remarks are made in Sec. V. Preliminary results of this work about some characteristics of the transition on smaller lattices were reported in Ref. 21.

II. FORMALISM AND SIMULATION

A. The model

The Hamiltonian of the quantum XY model we study in this paper is

$$H=-J\sum_{\langle ij\rangle}(S_i^xS_j^x+S_i^yS_j^y)\ , \tag{2.1}$$

where $\langle ij\rangle$ goes over all the nearest-neighbor pairs on the square lattice and S_i is the spin-$\frac{1}{2}$ operator. We would like to note that this model could be regarded as a special as of the more general quantum spin models

$$H=-\sum_{\langle ij\rangle}[J_\perp(S_i^xS_j^x+S_i^yS_j^y)+J_\parallel S_i^zS_j^z]\ , \tag{2.2}$$

when $J_\parallel=0$. This general anisotropic model describes a variety of magnetic systems. It is important to note, however, that a wide class of bosonic particle systems such as

$$H=\sum_{\langle ij\rangle}[-t(\psi_i^\dagger\psi_j+\psi_i\psi_j^\dagger)+Un_in_j] \tag{2.3}$$

can be mapped into the above anisotropic spin systems: the creation operator $\psi_i^\dagger\rightarrow S_i^x+iS_i^y$, and the density operator $n_i\rightarrow S_i^z+\frac{1}{2}$. The kinetic terms become the XY parts and the near-neighbor interaction potential terms become the Ising term, plus constants and $\sum_i S_i^z$, which is also a constant. This mapping makes the quantum spin models theoretically more interesting.

If the Ising coupling $J_\parallel$ is larger than the XY coupling $J_\perp$, at a temperature T very close to the critical point $k(T-T_c)\sim J_\parallel-J_\perp$, the discrete Ising components dominate and the general universality arguments suggest a critical behavior of the Ising type. This is indeed confirmed by a recent extensive study.[22] When the two couplings have exactly same strength, we have the isotropic Heisenberg model with an O(3) symmetry, there is no phase transition at any finite temperature.[16] In the most interesting case where the XY coupling is stronger, the O(2) symmetry would be dominant near T_c and the delicate Kosterlitz-Thouless transition occurring in 2D classical system would be the point of focus. To make things most clear, it is natural to set $J_\parallel=0$ and concentrate on the pure XY model. This is the approach taken in the present study. In the correspondent quantum bosonic system, this represents the extreme case where the near-neighbor hopping interaction is very strong, a case close to the situation in the high-T_c crystals.[1,2]

B. Quantum Monte Carlo

The quantum Monte Carlo method follows the Trotter-Suzuki transformation. The idea is to decompose the Hamiltonian into four parts[16] $H=H_1+H_2+H_3+H_4$ such that each H_i contains only terms commuting among themselves. Introducing a large number m of Trotter layers, such that $\Delta\tau\equiv1/mkT$ is small, one has the important factorization

$$e^{-(H_i+H_2+H_3+H_4)\Delta\tau}\simeq e^{-H_1\Delta\tau}e^{-H_2\Delta\tau}e^{-H_3\Delta\tau}e^{-H_4\Delta\tau}\ . \tag{2.4}$$

To simplify the notation, here and below, both the Boltzmann constant k and the exchange coupling J are set to 1. Thus, implicitly, energy is in units of J and temperature is in units of J/k. The partition function is

written as

$$Z=\mathrm{Tr}e^{-H/T}$$
$$=\mathrm{Tr}(e^{-\Delta\tau H})^m$$
$$=\sum_C \langle C_1|e^{-\Delta\tau H_1}|C_2\rangle \times\langle C_2|e^{-\Delta\tau H_2}|C_3\rangle\cdots\langle C_{4m}|e^{-\Delta\tau H_4}|C_1\rangle\ , \quad (2.5)$$

where we have inserted complete sets C_i of states (eigenstates of S_i^z). Because the terms within each H_i are commuting, each of the $4m$ short-time propagator $\langle C_t|e^{-\Delta\tau H_i}|C_{t+1}\rangle$ is further decomposed into product of two-spin propagators:

$$W=\langle S_{i,t}^z S_{j,t}^z|e^{-\Delta\tau(S_i^xS_j^x+S_i^yS_j^y)}|S_{i,t+1}^z S_{j,t+1}^z\rangle\ , \quad (2.6)$$

where t labels the $4m$ imaginary time slices of the m Trotter layers. Labeling the four states of the spin pair as $1=\uparrow\uparrow$, $2=\uparrow\downarrow$, $3=\downarrow\uparrow$, $4=\downarrow\downarrow$, the propagator can be written explicitly as

$$\underline{W}=\begin{bmatrix}1 & 0 & 0 & 0\\ 0 & \cosh(2K) & \sinh(2K) & 0\\ 0 & \sinh(2K) & \cosh(2K) & 0\\ 0 & 0 & 0 & 1\end{bmatrix} \quad (2.7)$$

with $K=\Delta\tau/4=J/4mT$. Since the matrix elements are all non-negative, they can be interpreted as transition probabilities, e.g., W_{23} is the probability for the state $\uparrow\downarrow$ at time slice t to transfer to state $\downarrow\uparrow$ at time slice $t+1$. Spin pairs at the two time slices forms a four-spin plaquette. The system, under this transformation, becomes a general $(2+1)$-dimensional Ising spin system with four-spin plaquette interactions specified in (2.5). We simulate the system using the Metropolis algorithm. Due to the conservation law of spin components, many elements of the transfer matrix are zero. To satisfy the conservation law, a set of four elementary updates of spins[16] are built into the algorithm which can generate all possible spin states. Besides two local updates, we also include the global updates along the time direction. The inclusion of global updates speeds up the thermal relaxation (sampling rate in the phase space) by about a factor of 3, and is also necessary for the global quantities, such as susceptibility. Periodic boundary conditions are imposed in all directions to preserve the translation invariance and to satisfy the trace requirement.

C. Observables

To calculate the average energy E, one writes[23] the matrix elements in W as a Boltzmann form $\exp(-\beta E_p)$ and associate the *effective* energy E_p with the four-spin plaquette configuration p. The partition function can be written as $Z=\sum_p \exp(-\beta E_p)$. Using $E=-\partial\ln(Z)/\partial\beta$, we have

$$E=\sum_p F_p e^{-\beta E_p}\equiv\langle F\rangle\ , \quad (2.8)$$

where the *thermal* energy F_p for the plaquette p is defined as

$$F_p=E_p+\beta\frac{\partial E_p}{\partial\beta}\ . \quad (2.9)$$

For example, the matrix element W_{22} corresponds to a plaquette $\begin{smallmatrix}\uparrow&\downarrow\\ \uparrow&\downarrow\end{smallmatrix}$, the associated effective energy $E_p=-T\ln[\cosh(2K)]$ and $F_p=-(J/2m)\tanh(2K)$.

Specific heat is calculated through the fluctuations: $C_V=\beta^2\partial E/\partial\beta$. From (2.9) we have

$$C_V T^2=\langle F^2\rangle-\langle F\rangle^2-\langle G\rangle\ , \quad (2.10)$$

where G_p, which arises due to the introduction of m Trotter layers, is given by $G_p=\partial F_p,\partial\beta$. For the example plaquette, $G_p=-(J/2m)^2\coth^2(2K)$.

The susceptibility for a quantum system is usually defined through the static response function

$$\chi_{A,B}=\frac{1}{\beta}\int_0^\beta dt\langle e^{tH}A^\dagger e^{-tH}B\rangle-\langle A^\dagger\rangle\langle B\rangle\ , \quad (2.11)$$

where A,B are operators. If A commutes with the Hamiltonian, as in all classical systems, this definition reduced to the standard form

$$\chi=\langle AB\rangle-\langle A\rangle\langle B\rangle\ . \quad (2.12)$$

Setting $A=B=\sum_i S_i^y$, we measure the (in-plane) susceptibility

$$\chi=\left\langle\left[\sum_i S_i^y\right]^2\right\rangle\Big/L^2\ , \quad (2.13)$$

where L is the linear size of the system. Note that we have omitted $\langle A\rangle^2$ because it is zero for any finite temperature, due to the Mermin-Wegner theorem. Since $\sum_i S_i^y$ does not commute with the Hamiltonian, χ differs from χ_A defined in (2.11). However, a rigorous inequality[13,24]

$$f(T)\le\chi/\chi_A\le 1 \quad (2.14)$$

exists where $f(T)$ is a function of T and can be evaluated in the Monte Carlo simulation. We found, as pointed out by De Raedt *et al.*, that $f(T)$ is always better than 99% when $T\ge T_c$. Thus, χ is a very good approximation of χ_A and in the following we will always refer to χ as the susceptibility.

The transverse spin-correlation function is defined on the in-plane component

$$C(r)=\frac{4}{L^2}\sum_n\langle S_n^y S_{n+r}^y\rangle\ , \quad (2.15)$$

where $n=(n_x,n_y)$, $r=(r_x,r_y)$, and the factor 4 is introduced such that $C(0)=1$. In simulation we only measure $C(r)$ for integer r and average along both the x and y directions.

When computing the transverse correlation functions, it is more convenient to work in the basis in which S^y is diagonalized. With this basis, the transfer matrix becomes

$$\underline{W}' = \begin{bmatrix} e^{K}\cosh(K) & 0 & 0 & e^{K}\sinh(K) \\ 0 & e^{-K}\cosh(K) & e^{-K}\sinh(K) & 0 \\ 0 & e^{-K}\sinh(K) & e^{-K}\cosh(K) & 0 \\ e^{K}\sinh(K) & 0 & 0 & e^{K}\cosh(K) \end{bmatrix} . \tag{2.16}$$

In this basis, the number conservation no longer exists and the winding number loses its meaning. Nevertheless, the global move along the t direction is still adopted for the purpose of speeding up the sampling rate.

D. Error controls and simulations

In the simulations, the systematic errors originated from the finite value of $\Delta\tau$ are kept very small. For small $\Delta\tau$, any thermal quantity A has the following expansion:[11]

$$A(\Delta\tau) = A(0) + a_2(\Delta\tau)^2 + a_4(\Delta\tau)^4 + \cdots \tag{2.17}$$

and is independent of volume because the error terms are proportional to the commutators between H_i. We used a large $m = 24$ for $T > 0.4$, so that

$$\Delta\tau \leq 0.1 \tag{2.18}$$

for all data points above T_c [All previous works used much larger $\Delta\tau$: $\Delta\tau = 0.25$ (Ref. 14) or much larger (Ref. 13).] We have also made explicit checks at several temperatures by using $m = 40$. Comparing with the $m = 24$ results, quantities such as E and C_V are indistinguishable, and the correlation functions are well within errors. At temperatures close to or below T_c, we increase m accordingly, typically keeping $\Delta\tau \leq 0.2$. Note that, at the lowest temperature point, $T = 0.05$, we used $m = 80$, which corresponds to $4 \times 80 = 360$ time slices. To ensure the needed accuracy, we typically repeat the simulation at smaller m and do an extrapolation based on (2.17).

An efficient multispin code which vectorized the local and global updates is used. The code was adopted[18] on the parallel hypercube computer. For this problem, the 32-node Caltech hypercube runs about eight times faster than the Cray Research XMP computer. To insure the accuracy of the results, high-statistics simulations are performed. We run two independent runs each of 6×10^5 sweeps on the 128×128 lattice, and at smaller length on smaller lattices at higher temperatures. These long runs are necessary because the autocorrelation time[25] τ_c, the time interval at which configurations are statistically independent, are typically 5000 sweeps for spin correlations at large distance (for local quantities such as E, the autocorrelation time is shorter). This is monitored by the autocorrelation function. τ_c is also useful in error estimates. Suppose the quantities are binned at 1000 sweeps each. We calculate both the standard deviation, σ, and τ_c on this data set. Then the error is given by $\sigma\tau_c^{1/2}$. In this way we avoid the question whether or not the bin size is large enough to ensure that data are statistically independent. We started at a higher temperature where the correlation length of the spin-correlation function are quite short so that no finite-size effects can arise. As T is lowered, we systematically increase the lattice size to satisfy

$$L \gtrsim 4\xi \tag{2.19}$$

(except at two points close to T_c, where the correlation length is so large that even on the large 96×96, 128×128 lattices, $L \simeq 3\xi$). Therefore, finite-size effects in our calculation are small. The fitting form (3.4), including the symmetric term to handle the periodic system, also helps eliminate the finite-size effects considerably. The smallness of the finite-size effects is evident in Fig. 3 where the scaled spin-correlation functions at different size lattices coincide very well. See Table I for parameters.

III. PHASE TRANSITION

A. Thermodynamic scaling

To address the issue of phase transition, we focus our attention to the scaling relations, the singular behaviors of the system near transition point, because their characteristics are the most clear signals to define and to classify the transition. Among the thermodynamic quantities, we first discuss the susceptibility, which typically exhibits strong divergent behavior that can be measured from experiments. The specific heat will be discussed in Sec. IV B because it is not divergent for this 2D system and therefore cannot serve as a signal for a phase transition.

The transverse susceptibility obtained in our simulations are listed in Table II. As T is lowered, χ increases very fast. From $T = 2$ to 0.7, it increases from 0.426 to 1.93, a factor of 4.5 increase. The rate of increase becomes much faster between $T = 0.7$ and 0.405, from 1.93 to 298, a factor of 154 increase. No any other thermodynamic quantities can change in such a rate. A divergent behavior is apparently developed. To find an analytical form of this behavior, we fit the data with

$$\chi = Ae^{B/(T-T_c)^{\nu}} . \tag{3.1}$$

This is the scaling form for the Kosterlitz-Thouless transition in the classical XY system, obtained by a renormalization-group analysis.[3] Here $\nu = \frac{1}{2}$, determined by the renormalization-group analysis. The constants A, B cannot be determined in this way and have to be fitted by experimental or simulational data. Our data fits the KT scaling very well: χ^2 per degree of freedom (DOF) is $6.1/(11-3) = 0.76$, which is shown in Fig. 1. The fitting result is

$$\begin{aligned} A_\chi &= 0.062(8) , \\ B_\chi &= 2.05(6) , \\ T_c &= 0.345(3) . \end{aligned} \tag{3.2}$$

TABLE I. A list of temperature, Trotter numbers, and lattice size used in the simulation and the energy and specific heat obtained. An asterisk indicates that extrapolations of Eq. (2.17) were made using several Trotter numbers, the largest m is listed in the table.

T	m	size	$-E$	C_V
2.0	16	16×16	0.1243(3)	0.0607(4)
1.5	16	16×16	0.1650(3)	0.1076(2)
0.9	16	24×24	0.2689(3)	0.283(3)
0.8	16	24×24	0.3003(3)	0.334(3)
0.7	24	24×24	0.3378(4)	0.418(1)
0.65	24	24×24	0.3560(3)	0.458(4)
0.6	24	32×32	0.3852(4)	0.532(1)
0.55	24	32×32	0.4133(4)	0.583(7)
0.52	24	48×48	0.4318(3)	0.596(6)
0.48	24	48×48	0.4579(4)	0.648(2)
0.45	24	64×64	0.4787(7)	0.651(1)
0.43	24	64×64	0.4906(2)	0.642(1)
0.42	24	96×96	0.4976(3)	0.616(2)
0.41	24	96×96	0.5046(2)	0.572(3)
0.405	24	128×128	0.5076(4)	0.576(9)
0.38	24	32×32	0.5177(7)	0.428(12)
0.35	24	48×48	0.5288(3)	0.284(22)
0.3	24	32×32	0.5391(3)	0.158(9)
0.25	32*	32×32	0.5455(4)	0.128(7)
0.2	32*	32×32	0.5500(2)	0.085(5)
0.15	32*	32×32	0.5519(2)	0.059(8)
0.1	48*	32×32	0.5525(2)	0.045(6)
0.05	80*	32×32	0.5553(2)	

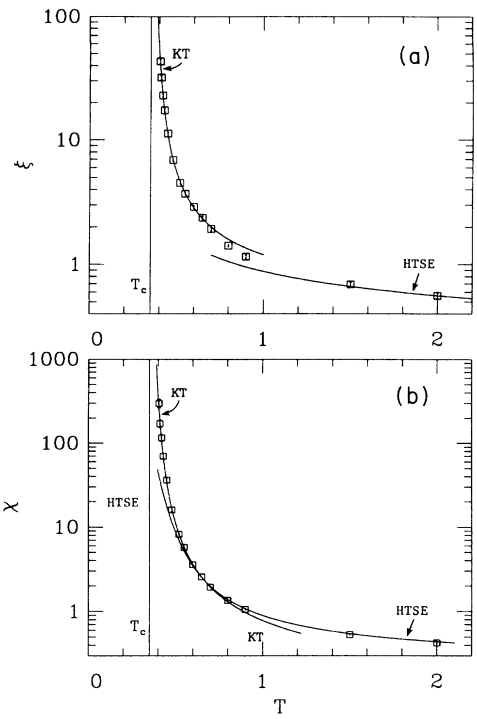

FIG. 1. (a) Correlation length measured. The curves for the KT scaling and a two-term HTSE are shown. (b) Transverse susceptibility measured. KT scaling and 12-order HTSE are also shown.

B. Correlation function

It is generally believed that the divergent correlation length is solely responsible for the divergent behaviors of the thermodynamical quantities such as the susceptibility. Correlation functions usually provide much insight to the system at the microscopic level. They are also of experimental interests because their Fourier transforms in k space, the structure factors, can be measured directly in scattering experiments.

The two-point transverse correlation spin correlations at several temperatures are shown in Fig. 2 and some short distance points are listed in Table III. As T is lowered, the spins become more strongly correlated. For example, at $T=0.405$, the correlation between two spins at a separation of $64a$ (a is the lattice spacing) is 0.055,

TABLE II. Correlation length, algebraic exponent, and transverse susceptibility obtained at different temperatures. χ_L is computed from correlation functions, Eq. (3.13), and χ' is the value after finite-size effects are corrected (see Sec. III D).

T	ξ	λ	χ	χ_L	χ'
2.0	0.56(4)	0.5	0.426(2)	0.426	0.426(2)
1.5	0.69(3)	0.5	0.531(2)	0.531	0.531(2)
0.9	1.16(4)	0.5	1.05(2)	1.05	1.05(2)
0.8	1.42(3)	0.5	1.34(2)	1.34	1.34(2)
0.7	1.88(7)	0.55(8)	1.93(2)	1.94	1.92(2)
0.65	2.41(8)	0.60(6)	2.56(3)	2.63	2.54(3)
0.6	2.90(8)	0.55(4)	3.58(4)	3.65	3.54(4)
0.55	3.70(9)	0.44(3)	5.72(11)	5.84	5.59(11)
0.52	4.53(8)	0.40(3)	8.22(2)	8.21	8.12(15)
0.48	6.92(14)	0.39(2)	16.0(7)	16.6	15.6(7)
0.45	11.3(2)	0.40(3)	36.3(1.4)	36.9	35.8(1.4)
0.43	17.4(5)	0.35(2)	70.1(5.6)	70.9	76.6(6.1)
0.42	22.9(6)	0.36(1)	116(11)	115	121(11)
0.41	30.0(1.5)	0.35(2)	171(18)	171	205(21)
0.405	43.4(2.2)	0.35(1)	298(35)	291	367(42)

about 10% of the correlation between nearest neighbors—the system has a large correlation length ξ. To quantitatively determine ξ, we fit the data points to a model correlation function. Far above T_c, the Ornstein-Zernike (OZ) theory predicts a form of $C(r)\sim r^{-1/2}e^{-r/\xi}$ for large r. Very close to T_c, the universal scaling of correlation function suggests that $C(r)\sim r^{-\eta}e^{-r/\xi}$, at large r, where η is the critical exponent, which is close to $\frac{1}{4}$ for the classical system in two dimensions (this is indeed accurate, as will be shown in Sec. III C). We therefore generalize the OZ form by introducing an algebraic exponent λ in the power-law part, i.e.,

$$C_\infty(r)=Ar^{-\lambda}e^{-r/\xi}, \tag{3.3}$$

for an infinite lattice. In practice, for a $L\times L$ system with periodic boundary condition, we fit to

$$C_L(r)=A[r^{-\lambda}e^{-r/\xi}+(L-r)^{-\lambda}e^{-(L-r)/\xi}]. \tag{3.4}$$

The fits to this form are excellent, as shown in Fig. 2. At higher T, $\lambda\approx 0.5$, as expected. When T is lowered down towards T_c, we find that λ slightly shifts down in a systematical way, to about 0.35. This gradual decrease in λ with lowering T is consistent with our expectation that λ should approach the critical exponent $\eta\sim\frac{1}{4}$. The surprisingly good fit to (3.4) even for data points with $r\lesssim\xi$ suggests that the power-exponential form (3.3) is a general form for correlation functions.

The best fits are listed in Table II. As shown in Fig. 1(a), ξ increases very fast as T is lowered. From $T=2$ to 0.405, ξ increases from $0.56a$ to $43a$, a factor of 78 increase. Clearly, ξ will diverge at some finite T_c. The intimate relation between χ and ξ suggests that ξ once again should follow a Kosterlitz-Thouless thermodynamic scaling

$$\xi=Ae^{B/(T-T_c)^\nu},\quad \nu=\tfrac{1}{2}. \tag{3.5}$$

In the fit we include all 11 data points whose $\xi\geq 1.9a$, which we consider to be the region where cooperative phenomena takes place and the singular behavior of (3.5) is dominant. From $\xi=1.93a$ to $43.4a$, the correlation length increases by factor of 23, thus these 11 points cover a substantial part of the critical region and the fit should be fairly reliable. The fit is indeed very good: χ^2 per degree of freedom is $7.7/(11-3)=0.96$, which is also evident in Fig. 1(a). The parameters of the fit are

$$\begin{aligned} &A_\xi=0.285(27),\\ &B_\xi=1.14(5),\\ &T_c=0.353(3). \end{aligned} \tag{3.6a}$$

The important fact here is that the T_c determined from fitting ξ is very close to the T_c obtained from fitting χ. (After finite-size effects are corrected for χ, the T_c obtained from fitting χ moves up and almost coincides with that from ξ, see Sec. III D.) The good quality of the fits to the KT scaling and the closeness of T_c's obtained are rather strong evidence of a Kosterlitz-Thouless phase transition.

As further evidence for a KT transition, we note that the specific heat exhibits a finite peak at a temperature above T_c (see Sec. IV B), similar to the situation in the classical model. In addition, the "derivative of helicity

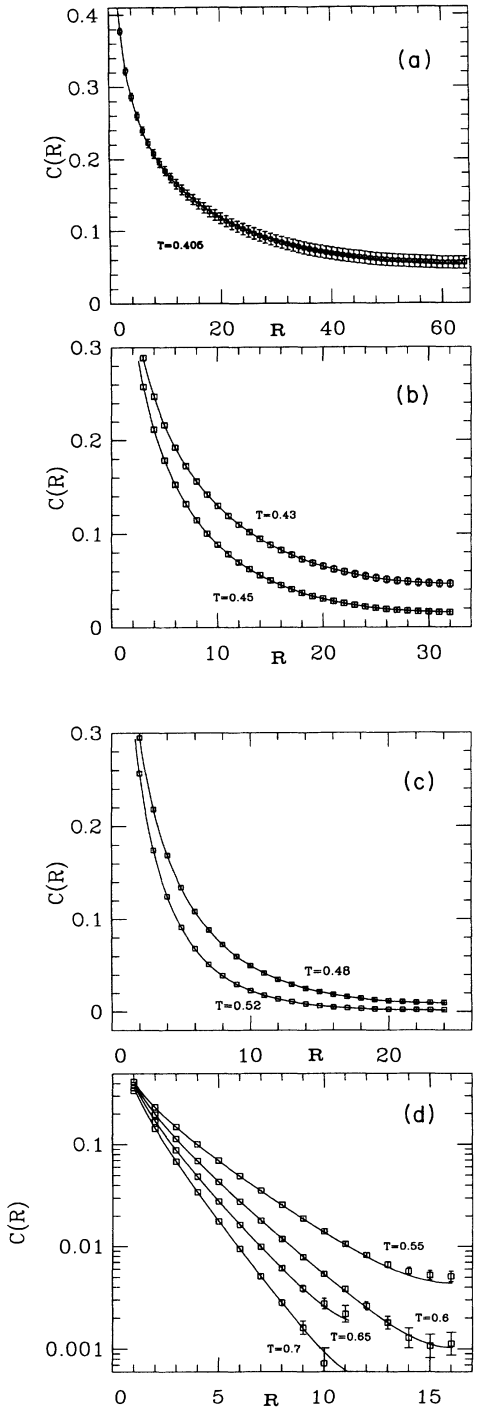

FIG. 2. Correlation functions measured. (a) at $T=0.405$ on the 128×128 lattice, (b) at $T=0.43$, 0.45 on the 64×64 lattice, (c) at $T=0.48$, 0.52 on the 48×48, lattice and (d) at $T=0.55$, 0.6, 0.65, 0.7. Correlations at $T=0.41$, 0.42 on the 96×96 lattice have been shown in Ref. 21.

TABLE III. Longitudinal (upper half) and transverse (lower half) correlation functions at several temperatures. Both are normalized to one at $r=0$.

T	$r=1$	$r=2$	$r=3$	$r=4$
0.55	−0.114 5(1)	−0.001 6(1)	−0.000 2(1)	−0.000 06(10)
0.45	−0.135 3(2)	−0.003 0(1)	−0.000 7(1)	−0.000 02(10)
0.35	−0.151 6(2)	−0.005 1(2)	−0.001 2(2)	−0.000 09(15)
0.2	−0.164 7(1)	−0.007 3(1)	−0.002 7(1)	−0.000 67(10)
0.1	−0.167 2(1)	−0.008 6(1)	−0.003 5(1)	−0.001 10(09)
0.55	0.414 4(7)	0.232 5(6)	0.148 9(5)	0.100 3(5)
0.45	0.477(2)	0.327(2)	0.257(2)	0.212(2)
0.35	0.53(2)	0.43(2)	0.40(2)	0.38(2)
0.2	0.55(2)	0.46(2)	0.44(2)	0.43(3)
0.1	0.55(2)	0.47(3)	0.45(3)	0.44(3)

modulus" exhibit a similar finite peak[14] above T_c (in the classical case, such a peak has been suggested[8] as a good signal for the KT transition because its dependence on system size is stronger than that of the specific heat). Another signal is from the local vortex density, which is also a quantum analog of the classical model, although the analog is not quite as clear. At higher T, one expects a larger vortex density because of the separation of the vortex-antivortex pairs. At low T, the vortex-antivortex binds together, one expects a small vortex density. Near T_c, one expects a rise of vortex density. Indeed, De Raedt *et al.*[13] observed a rise near $T=0.56$ while Loh *et al.*[14] observed a rise at $T=0.35$–0.4, quite consistent with our value $T_c=0.353$.

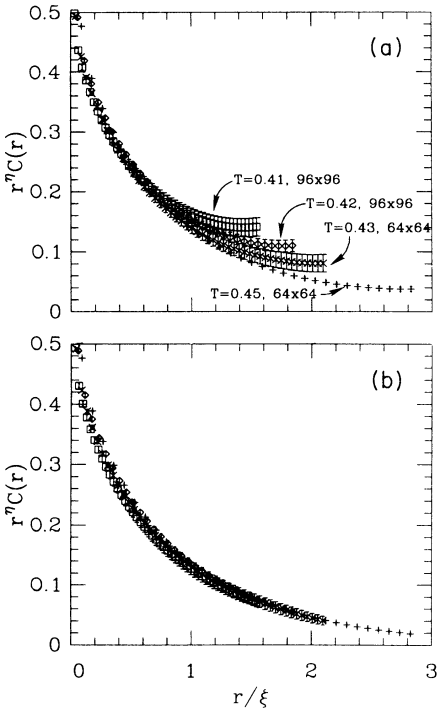

FIG. 3. Scaling of correlation functions. (a) Data directly measured. (b) Same data, but the finite-size effects are corrected.

C. Universal scaling of the correlation functions

For the critical phenomena discussed here, it is generally believed that the correlation length is the only relevant length scale. The universal scaling of the correlation function further suggests that, near T_c,

$$C(r)=\text{const}\times r^{-(d-2+\eta)}D(r/\xi)\ , \tag{3.7}$$

where $d=2$ is the dimension. This was first proposed[26] in analyzing the Ising model using the block spin idea which was later developed into real-space renormalization (see Ref. 27 for a general review). Note that this is not an asymptotic relation, it is supposed to hold for any r. This relation also serves as the definition of the critical exponent η.

We now examine this scaling relation using the correlation functions measured in the simulation. To this end, we define a scaling invariant,

$$S(x)\equiv r^{\eta}C(r)\ , \tag{3.8}$$

where $x=r/\xi$. For each T, from the correlation function, $S(x)$ defines a set of data with errors. $S(x)$ should be independent of T if the scaling holds. In Fig. 3 we plotted $S(x)$ at four temperatures, using $\eta=\frac{1}{4}$. In Fig. 3(a), we use the $C(r)$ directly obtained in the simulation. At small x, the four data sets are rather close, but as $r\to L/2$, each data set flattens, the four data sets separated. However, since the lattice sizes at all temperatures are finite, the finite-size effects may cause these deviations. The finite-size effects can be easily eliminated. Given the excellent fit of $C(r)$ to (3.4) as evident in Fig. 2, the finite-size effects represented by the boundary effects can be accurately estimated from (3.4). Writing (3.4) as $C_L(r)=C_\infty(r)Z(r)$, we see that the boundary effects are absorbed into a multiplicative factor, $Z(r)$, which can be computed using the fitted λ,ξ as

$$Z(r)=1+\left[\frac{r}{L-2}\right]^{\lambda}e^{-(L-2r)/\xi}\ . \tag{3.9}$$

Eliminating this factor from the measured correlation function, we obtained the corrected correlation function

$$C'(r)=C(r)/Z(r)\ . \tag{3.10}$$

The resulting corrected data sets collapse to a single curve, as shown in Fig. 3(b). This indicates that the correlation functions in this *quantum* transition satisfy the *classical* universal scaling with the critical exponent $\eta=\frac{1}{4}$. It also demonstrates that our method of handling periodic boundary conditions eliminates the finite-size effects.

From the universal scaling, one can easily obtain the usual scaling relation among the susceptibility, the correlation length, and the exponent η:

$$\chi=\sum_{\mathbf{r}}\langle S_{\mathbf{0}}^{y}S_{\mathbf{r}}^{y}\rangle=\tfrac{1}{4}\int_{0}^{\infty}C(r)2\pi r dr=\text{const}\times\xi^{2-\eta}\ , \quad (3.11)$$

near transition point, using (2.13), (2.15), and (3.7). We can estimate η from the scaling behaviors of χ,ξ of (3.1) and (3.5) to obtain

$$\eta=2-B_{\chi}/B_{\xi}\ , \quad (3.12)$$

assuming the T_c's determined from fitting χ,ξ coincide. Using this relation, a rough estimate using the fitted parameters in (3.2) and (3.6) gives

$$\eta=2-2.05(6)/1.14(5)=0.29\pm0.09\ ,$$

in agreement with $\eta=\frac{1}{4}$ for the classical case. This is a further consistency check. (For a more accurate value, see the next section.)

D. Scaling of the corrected χ

The significant reduction of finite-size effects in correlation functions discussed in the previous section suggests that the same method can be applied to other interesting quantities. We have examined susceptibility because it can be written as a direct sum over all correlation functions, see (3.11). Equation (3.11) also suggests that the finite-size effect on χ could be large because $C(r)$ in the large-r region are weighted more and in this region the finite-size effects on $C(r)$ are appreciable, as evident in Fig. 3.

An important consistency check is to compute χ through (3.11) using the correlation functions we obtained. This microscopically computed quantity should be same as the macroscopic quantity defined in (2.13). To compute the sum over correlation functions, we use the isotropic nature, $C(\mathbf{r})=C(r)$, so that only the on-axis correlations are needed now. We further simplify the discrete sum to a sum in radial direction:

$$\sum_{r_x=1}^{L}\sum_{r_y=1}^{L}f(r)=\sum_{r=0}^{R}2\pi r f(r)\ .$$

For the $L\times L$ lattice, the upper limit R of the sum is determined by $\pi R^2=L^2$. The results computed in this way,

$$\chi_L=(\pi/2)\sum_{r=0}^{R}rC_L(r)\ , \quad (3.13)$$

using the fitted parameter A,λ,ξ at each T, are listed in Table II [for ≥ 0.8, ξ is short, $C(r)$ falls very rapidly, the finite-size effects are very small; we instead compute the second expression in (3.11) using $C(r)$ directly measured]. The agreements with the macroscopic results are excellent.

The infinite lattice results could now be computed as $\chi_\infty=(\pi/2)\sum_{r=0}^{\infty}rC_\infty(r)$, using the same A,λ,ξ. However, to be consistent, we treat the ratio $Z_\chi=\chi_\infty/\chi_L$ as the *correction* factor due to the finite size. The final value for infinite lattice is the direct results corrected by this factor:

$$\chi'=Z_\chi\chi\ . \quad (3.14)$$

The results are listed in Table II. From Table II we see that, for $T\geq 0.45J$, the corrections are very small. This indicates that, for an $L\times L$ lattice with $L/\xi\geq 5.6$, the finite-size effects are essentially negligible. However, these effects could be as large as 20% for lattices with $L/\xi\simeq 3$. We note that χ has the most severe finite-size effects due to the long-range nature, whereas local quantities such as E and C_V, are much less sensitive to the size of the system.

We expect that the corrected χ will fit the KT form better. Indeed, the quality of the fit is improved significantly: $\chi^2/\text{DOF}=0.38$, reduced by half. The fit gives

$$\begin{aligned}A_\chi&=0.0785(7)\ ,\\ B_\chi&=1.89(6)\ ,\\ T_c&=0.354(3)\ .\end{aligned} \quad (3.6b)$$

This T_c almost coincides with that obtained from ξ, reflecting the intimate relationship between correlation function and the susceptibility. The significant enhancement due to the finite-size correction on χ is not entirely unexpected, since the finite-size correction on ξ's are already handled by the boundary reflection in the fitting form (3.4). Nevertheless, it is a good indication that our method of handling finite-size correction is both consistent and accurate.

We can now use the scaling relation (3.11) to compute the exponent η. Using (3.12) we would get $\eta=2-1.66(9)=0.34\pm0.09$, with a fairly large error. A more accurate way is to look at the scaling relation directly, i.e., the plot χ' versus ξ on a double-logarithmic scale, shown in Fig. 4. The linear relation is very clear. The slope is $2-\eta=1.724(14)$. This gives the most accurate estimate

$$\eta=0.276\pm0.014 \quad (3.15)$$

in this paper, although it lies slightly away from the expected 0.25.

E. Finite-size scaling at T_c

The above determinations of η are made from data in the transition region at $T>T_c$. One can also obtain η directly at $T=T_c$ by measuring correlation functions and susceptibility. In practice, this is much harder because the fluctuation is very large due to the fact ξ is infinite. Our earlier criterion of using a lattice with $L\gtrsim 4\xi$ cannot be used, and we employ a popular method, the finite-size

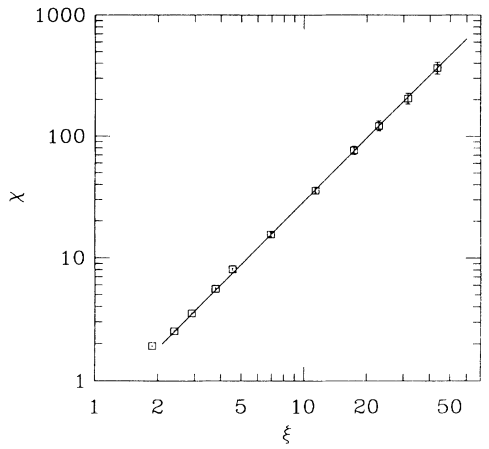

FIG. 4. log-log scaling plot between χ,ξ; see (3.11).

scaling. At T_c, we simulated lattices of sizes 16×16, 24×24, 32×32, and 48×48. A rough estimate can be obtained directly from the correlation functions at the 48×48 lattice, even though the lattice may be barely large enough to see the power-law falloff. Now $C(r)\sim r^{-\eta}$ for large r. Treating the periodic boundary condition as before, we fit the correlation function data to

$$C_L(r)=A[r^{-\eta}+(L-r)^{-\eta}] . \tag{3.16}$$

$C(r)$ and the fit are plotted in Fig. 5. Except the $r=1$ point, the fit is quite good. The powerlaw falloff is seen reasonably well (the flattening of the data at larger r is due to the boundary reflections which is particularly strong in this case because $\xi=\infty$). The fitted parameters are $A=0.37(6)$ and $\eta=0.27(5)$. This η agrees well with our earlier analysis. The relatively large errors in these parameters are the reflection of large errors in the correlation function obtained, which is, in turn, a result of the large fluctuations of the system at the critical point.

In the finite-size scaling analysis, one sets $\xi=L$ because, for a finite system of linear size L, the correlation length cannot be longer than L, even though ξ is infinite for an infinitely large system. From the relation (3.11) we now have

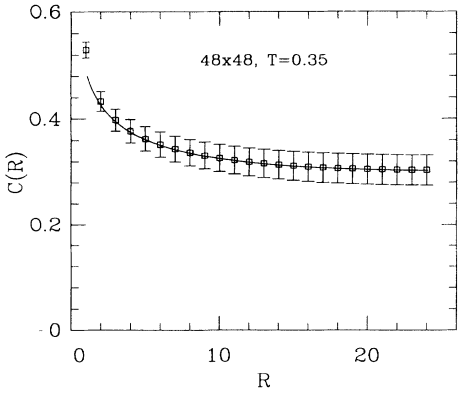

FIG. 5. Correlation function at T_c. The curve is the fit to (3.16).

$$\chi=\text{const}\times L^{2-\eta} . \tag{3.17}$$

Fitting $\ln(\chi)$ obtained on these four lattices as a function of $\ln(L)$, we obtained a straight line with a slope $2-\eta=1.75(7)$. The data (in logarithmic scale) and the fit are shown in Fig. 6(a). The scaling relation is satisfied quite well. From this result, we obtain independently $\eta=0.25(7)$. Another independent fit can be made on the quantity $C(r=L/2)$, i.e., the correlation function at half-lattice size, the maximum distance on the periodic lattice. From (3.16), $C(L/2)$ has a scaling relation

$$C(L/2)=\text{const}\times L^{\eta} . \tag{3.18}$$

$C(L/2)$ obtained on the four lattices and the fit are shown in Fig. 6(b). The fit is reasonably well, the slope gives $\eta=0.249(76)$.

Although these results about η have relatively larger errors, they are obtained in quite different ways and they agree very well with each other and with our earlier result (3.15). This fact, therefore, provides a substantial confirmation to our previous conclusion that $\eta=\frac{1}{4}$.

F. Universality and quantum effects

We have identified the scaling behaviors of the phase transition of the quantum system. The scaling behaviors of the susceptibility and correlation length are characteristic of the KT transition in the classical case. This suggests that, although quantum effects at finite T can change the quantitative behavior of these spin systems with *continuous* symmetries, the qualitative scaling picture of the classical system persists. This is the main conclusion of the present study. This conclusion could be qualitatively understood following the general universali-

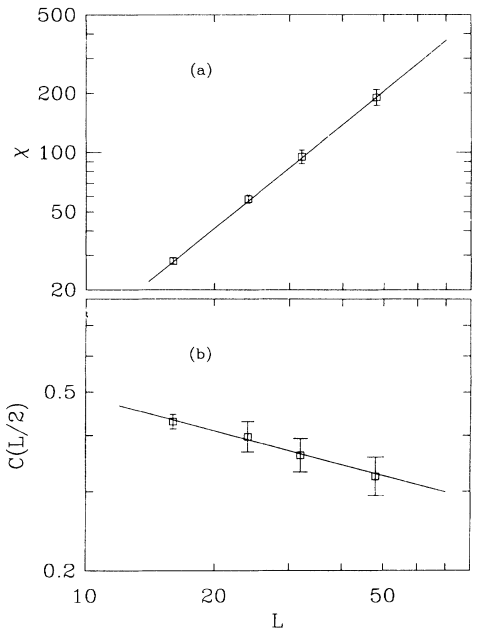

FIG. 6. Finite-size scaling. log-log plots of (a) ξ vs L and (b) $C(L/2)$ vs L. See (3.17) and (3.18).

ty arguments: the dominant behavior of the system near the critical point is determined by long-range fluctuations which are characterized by symmetries and dimensionality and are independent of details of the interactions. The quantum effects may change the short-range fluctuations which can be integrated out and enter the picture as renormalizations of the physical parameters. For example, quantum fluctuations are capable of pushing the transition point from $T_c=0.898$ in the classical model down to $T_c=0.353$ in the quantum case, although not strong enough to push it down to zero. They also reduced (renormalized) the constant B_ξ from 1.67 in the classical case to 1.14 in the quantum case.

A distinctive quantum effect arises due to the differences regarding the spin space. In the classical case, the spins are confined to the X-Y plane (thus, the model is conventionally called a "planar rotator" model). This is important for the topological order in KT theory. The quantum spins are not restricted to the X-Y plane, due to the presence of S^z in the commutator relation. The KT behavior found in the quantum case indicates that the quantum effects due to the extra S^z dimension in the spin space (which does not appear in the Hamiltonian) is not important, in fact, as far as critical scaling behaviors are concerned. This interpretation is supported by the behavior of the correlation functions between S^z components listed in Table III. At nearest neighbors, these longitudinal correlations, $C^z(r)\equiv\sum n 4\langle S_n^z S_{n+r}^z\rangle/L^2$, have some appreciable values, ~ -0.16, although about five times smaller than the transverse correlations. But, for $r\geq 2$, $C^z(r)$ drop off very rapidly, by orders of magnitude. They are very weak and short ranged. Even at a temperature as low as $T=0.1J$, where the correlations are expected to be large, $C^z(r)$ is 2 orders of magnitude smaller than $C(r)$ and has a correlation length less than lattice spacing, while $C(r)$ has an infinite correlation length.

From the universality point of view, the more accurate classical equivalent of the quantum XY model should be the model where the classical spins can point to any direction in 3D. In this "3D rotator" model, $C^z(r)=0$, because a flip of sign of S^z costs no change in energy. Therefore, the thermal fluctuation is dominated by the transverse components—we expect an identical KT behavior, except that T_c could be pushed down slightly.

It is interesting to note that the nearest-neighbor S^z correlation is negative, so that S^z behaves like an antiferromagnet (the next-nearest-neighbor correlation is 10 times smaller and has no effects to this discussion). This fact can be traced back to the simplest XY system where only two spins are present. In that case, the correlation is -1. When many other spins join the system, this nearest-neighbor correlation persists, even though the strength is reduced.

Due to the correlations between S^z, the longitudinal susceptibility $\chi_l=\langle(\sum_i S_i^z)^2\rangle/T$ does not vanish, unlike that in the classical case. However, because of the weak correlations, χ_l remains a small quantity in the whole temperature range, as shown in Table IV. The antiferromagnetic correlation between S^z makes the staggered longitudinal susceptibility, $\chi_l^\dagger=\langle(\sum_i \varepsilon_i S_i^z)^2\rangle/T$, where $\varepsilon_i=\pm 1$ depends on the sublattice, greater than χ_l. As $T\to 0$, χ_l remains finite, whereas $\chi_l^\dagger$ is expected to diverge.

TABLE IV. Longitudinal susceptibility χ_l and staggered longitudinal susceptibility $\chi_l^\dagger$ at several temperatures.

T	χ_l	$\chi_l^\dagger$
0.45	0.680(7)	0.972(9)
0.35	0.636(8)	0.901(14)
0.2	0.626(12)	0.922(9)
0.1	0.505(58)	0.926(8)

In general, universality implies that different systems have qualitatively the same scaling behaviors near critical temperature. A stronger form of universality expects that the scaling behaviors are characterized by exactly the same critical exponents for different systems. Indeed, the critical exponents of the quantum XY model are the same as those of the classical model. First we note that the exponent η in the two cases are same. Although our value seems to be slightly higher than $\frac{1}{4}$, the spin-wave results for the classical model,[3] extensive Monte Carlo studies in the classical case,[7] suggest that η is possibly slight higher than $\frac{1}{4}$.

Perhaps the more interesting exponent is ν. In principle, ν in (3.5) could differ from its classical value $\frac{1}{2}$. Our data are sufficient to detect any systematic deviation from this value. For this purpose, we made several tests. The simplest test is to write (3.5) in the form

$$\ln(\xi)=\ln(A)+B/(T-T_c)^\nu,\quad \nu=\tfrac{1}{2}\ . \tag{3.19}$$

In this form, it is clear that, given T_c, $\ln(\xi)$ should become a linear function with respect to $x=(T-T_c)^{-1/2}$, independent of the values of A,B. This is indeed the case, as plotted in Fig. 7. As expected, data points all fall well on a straight line (except the point at $T\gtrsim 0.7$, where the critical region presumably ends). A systematic deviation from $\nu=\frac{1}{2}$ would lead to a slightly curved line instead of a straight line. The next test is to let ν vary as a

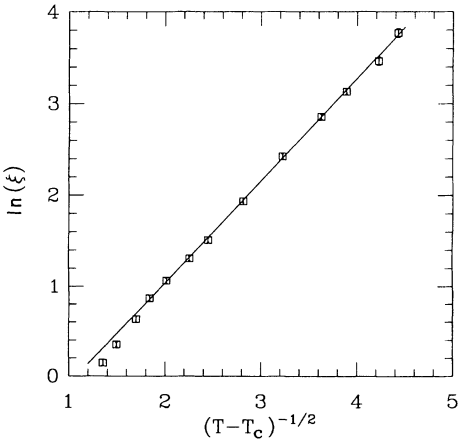

FIG. 7. A plot to examine the exponent ν.

free parameter in the fits. In this way we can obtain lower and upper bounds for ν. The result of fitting correlation length is

$$\nu_\xi = 0.488^{+0.1}_{-0.02} . \tag{3.20}$$

We note that these bounds are not errors in the usual sense. They are obtained in the following way. We fix $\nu=\nu_0$ and fitting the other three parameters, A, B, T_c to minimize the usual χ^2. The minimum χ^2 thus obtained is a function of ν_0: $\chi^2(\nu_0)$. At $\nu_0=0.488$, $\chi^2(\nu_0)$ reaches the minimum. The bounds are determined by varying ν_0 slowly up or down until we reach a $\chi^2(\nu_0)$, which is greater than $\chi^2(0.488)$ by 1. Similarly, we obtain the bounds for ν by fitting the susceptibility

$$\nu_\chi = 0.495^{+0.1}_{-0.04} . \tag{3.21}$$

These bounds strongly support our conclusion that $\nu=\frac{1}{2}$ for the quantum model.

G. The width of transition

How wide is the critical region ΔT where the scaling laws dominate the behaviors of the system? This is an interesting issue for theory, and an practical one for experiments. Figure 1 indicates $\Delta T \approx 0.3J$. Since $T_c=0.35J$, $\Delta T/T_c \simeq 0.8$, this transition region is considered to be wide. This is a special feature occurring in two dimensions due to the large thermal fluctuations. We note that, for the classical XY model,[7] $\Delta T \approx 0.56$, $T_c=0.9$, and $\Delta T/T_c \simeq 0.6$. The quantum XY model has a wider $\Delta T/T_c$ than the classical model because of the additional quantum fluctuations. For the quantum Heisenberg model $T_c=0$, since the system becomes ordered at $T=0$ from a disordered state at $T>0$. The $T=0$ behavior is found to extend to $T \approx J$ for the spin-$\frac{1}{2}$ antiferromagnetic system[16] and to $T \approx 2J$ for the spin-1 system,[28] corresponding to $\Delta T/T_c=\infty$.

These 2D phenomena are in sharp contrast with those 3D transitions. Typically in 3D, the transition is quite sharp and T_c is usually quite high, $T_c \gtrsim 3J$. The transition region is quite narrow, $\Delta T/T_c \sim 10\%$.

The surprising difference, however, is really on the macroscopic level, without refering to the details of the interactions. Experimentally we have only one temperature scale for the system, namely, T_c, and the width of transition region is measured in terms of T_c. Microscopically, the exchange coupling J is a more fundamental temperature scale. In terms of J, ΔT is not much different from $\Delta T \sim 0.6J$ in the 2D cases to $\Delta T \sim 0.3J$ in 3D cases. This factor of 2 difference could be attributed to the larger fluctuations in two dimensions. The real big change is T_c, $T_c=0$ in one dimension for all spin models. $T_c=0$ for all models with O(N) symmetry with $N \geq 3$ in two dimensions, and $T_c \gtrsim 3$ for the same models in three dimensions.

In general, the correlation length at different temperatures is a good basis for judging how wide the transition region is. For models lacking other characteristic lengths, the lattice spacing a serves as an important length scale. When the correlation length becomes larger than a, e.g., $\xi \gtrsim 3a$, the cooperative phenomenon should take place. This simple criteria works for all above cases. This fact also explains why a lattice as small as 12×12 (or even 8×8) can develop signals of a phase transition, as many early computer-simulation studies demonstrated. Therefore, correlation lengths provide much insights to the system and is a better criterion than the ratio $\Delta T/T_c$.

IV. THERMODYNAMICS

A. Energy

We start at high temperatures because a high-temperature series expansion (HTSE) has been calculated[5,9] which we can compare with. The obtained energy is listed in Table I and is also plotted in Fig. 8. The data show that E is a monotonic increasing function as T increases. This is expected theoretically because its derivative, the specific heat, is always positive:

$$C_V = d\langle E\rangle/dT = (\langle E^2\rangle - \langle E\rangle^2)/T^2$$

when working with the eigenstates of the Hamiltonian. We note that, as indicated in (2.10), this positivity is not obvious when the Trotter layers are introduced, because $\langle G\rangle$ is not always positive. Therefore, the monotonic increase of E in the data is an good confirmation of the Trotter-Suzuki approach. To compare with the 13th-order HTSE results of Rogiers *et al.*,[9(a)]

$$E(T) = -\frac{1}{2}\left[x - \frac{0.5}{3!}x^3 - \frac{11}{5!}x^5 + \frac{743.75}{7!}x^7 - \frac{55\,374}{9!}x^9 + \frac{4\,404\,418}{11!}x^{11}\right], \tag{4.1}$$

where $x=J/2T$, we plotted this curve in Fig. 8. The agreement is excellent for $T \geq 0.6$.

At very low temperature, i.e., near $T=0$, the asymptotic behavior of E is expected to be a form of

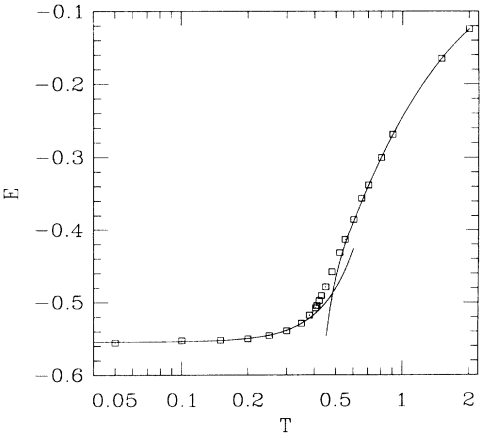

FIG. 8. Energy density per site. The 12-order HTSE result is shown at the high-T region and the T^3 behavior is shown in low-T region. T is in log scale to emphasize the low-T fit.

$E_0+\text{const}\times T^{\alpha}$. Therefore, we fitted data to such a form. The best fit is found to be

$$E(T)/N=-0.5543(1)+0.594(35)T^3 , \tag{4.2}$$

where the numbers in parentheses are errors in the fit. This is shown in Fig. 8 as the curve in the low-T region. The fit is very good. This T^3 behavior indicates that the excitation spectrum of the many-body system is linear in momenta, $E(k)\sim k$ at $T\sim 0$, in agreement with the spin-wave analysis.[19] The validity of the spin-wave treatment in the topological order phase indicates that the spin-wave treatment does not necessarily require a long-range order in which all spin align up in the particular direction. The extrapolated ground-state energy $E_0=-0.5543(1)$ agrees with both the spin-wave result -0.54 and the finite cluster calculation[20] -0.554.

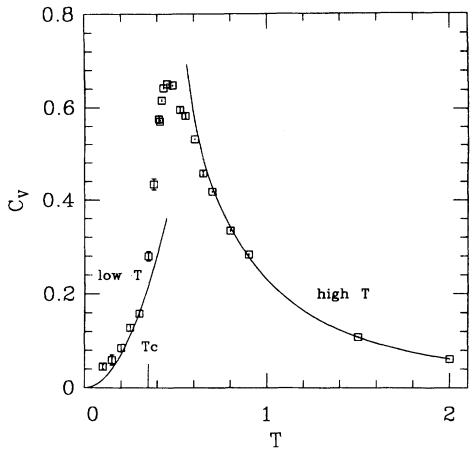

FIG. 9. Specific heat. Two curves shown are the derivatives of the corresponding curves in Fig. 8.

B. Specific heat

Specific heat computed through (2.10) are listed in Table I and plotted in Fig. 9. In the high-T region, we plotted the HTSE results [the temperature derivative of the energy of (4.1)]. The agreement between our data and the HTSE results is quite well for $T\geq 0.8$. Note that our C_V is obtained by measuring the fluctuations in the energy, whereas the HTSE results is the energy derivative.

At very low T, the low acceptance rate in the Monte Carlo sampling makes it quite difficult to determine C_V accurately, resulting larger relative errors in Table I. The accurate results can be obtained, however, by the simple derivative of energy at this region, $C_V=dE/dT$, because energy is much more accurately measured. Taking derivative of (4.2), we have

$$C_V(T)/kL^2=1.78(11)T^2 . \tag{4.3}$$

This is plotted in Fig. 9. The Monte Carlo data obtained by measuring the fluctuations (in Table I) are consistent with this curve up to $T\approx 0.4$, similar to that of E. The lowest points $T=0.05$ and 0.1 are off slightly, which is not unexpected at such an extremely low temperature.

In the transition region, as clearly seen in Fig. 9, the specific heat has a distinctive λ-shape finite peak at around

$$T_m=0.45J . \tag{4.4}$$

The peak clearly shifts away from $T_m=0.52$ on the much smaller 8×8 lattice.[14] The height of the peak, however, remains the same,

$$C_V^m/L^2k=0.65 , \tag{4.5}$$

in agreement with Loh *et al.*[14] De Raedt *et al.*[13] suggested a logarithmic divergent C_V, which, in our opinion, is very likely an artifact due to the small-m values used in their work. The shape of the curve is asymmetric near the peak. These features of the C_V curve differ from that in the classical XY model.

One striking feature in Fig. 9 is a very steep increase of C_V at $T\approx T_c$, raising the possibility that the transition in the quantum XY model is not only KT-like, but also a third-order transition. This has prompted us into further investigation by simulating larger systems near T_c. This result is negative: (1) The statistical fluctuations are very large, it is larger on a 48×48 lattice than on the 32×32 lattice (a signal of this is the larger errors of C_V around T_c, see Table I). (2) To the extent that our statistics can determine, the slope of the C_V curve is quite stable, we did not notice any clear changes. The negative conclusion could be explained by the thermodynamic scaling theory of the free energy,[27] i.e., the singular part of the free energy near T_c is

$$F_{\text{sing}}\sim\xi^{-d}\sim\exp(-dB_{\xi}/\sqrt{T-T_c}) . \tag{4.6}$$

So all the temperature derivatives of the singular part at T_c must be zero because of the exponential diminishing factor. Therefore, the scaling of free energy directly implies the nondivergent behavior of C_V in the KT transition. It appears that the nonsingular parts in the free energy cause C_V to exhibit a sharp rise near T_c, just as it exhibits a finite peak near $T=0.45$. We note that a finite C_V peak also occurs in the isotropic Heisenberg model.[16]

C. Susceptibility

The in-plane susceptibility χ has been plotted in Fig. 1(b). It diverges in the critical point as being analyzed in Sec. III. As temperature rises up from T_c, χ drops off quickly. We now compare our data with the 12-order HTSE result

$$\chi(T)=\frac{1}{4}\left[1+2x+3x^2+\frac{20}{3!}x^3+\frac{78}{4!}x^4+\frac{393}{5!}x^5+\frac{2470}{6!}x^6+\frac{17\,095.5}{7!}x^7+\frac{124\,952}{8!}x^8+\frac{990\,057}{9!}x^9+\frac{8\,892\,804}{10!}x^{10}+\frac{90\,111\,673.5}{11!}x^{11}+\frac{963\,803\,726}{12!}x^{12}\right] . \tag{4.7}$$

[In the definition of Rogiers *et al.*[9(a)] $\chi=(\sum S^y)^2/TL^2$, which differs from ours by the factor $1/T$, and their Hamiltonian $H=\sum 2J(S_i^xS_j^x+S_i^yS_j^y)$ also differs from ours by a factor of 2. These differences in definition have been corrected in (4.1) and (4.7) such that all results now conform to our definitions.] As is clearly seen in Fig. 1(b), the HTSE results agree very well with our data from high T all the way down to $T\approx 0.6$.

We note that χ remains *infinite* at all temperatures below T_c, an unusual feature of the KT transition. The situation is similar to the classical XY model, where there exists a line of fixed points in the renormalization-group equations. In real space, this means that the system remains at critical states at all temperatures below T_c. Although the system is displaying topological order, those large scale patterns induced by the isolated vortice-antivortice pairs, it is disordered in the usual sense that no spin alignment along a particular direction occurs, i.e., $\sum_i \langle S_i^y \rangle = 0$. However, the two-point correlation functions falls off only algebraically so that $\sum_i \langle S_0^y S_i^y \rangle$ diverges. The infinite χ suggests that the system is not stable, any small external magnetic field could cause spin alignment, establishing a long-range order. This effects of infinite susceptibility make it difficult to determine experimentally whether a particular ordering transition is of the KT type or of the conventional type. Of course, there are other characteristics of the KT transition which can be measured experimentally, the spin stiffness, for example.

V. SUMMARY

We have carefully examined various scaling behaviors of the quantum XY model near the critical temperature. We have shown fairly convincing evidences that the Kosterlitz-Thouless phase transition originally discovered in the classical XY model also takes place in the quantum model. Furthermore, the critical exponents are found to be in very good agreements with those in the classical model. The problem associated with the third components in spin space is clarified and the universality is established in this delicate transition in two dimensions.

ACKNOWLEDGMENTS

I wish to thank Miloje Makivic for the collaboration at the early stage of this project. The support from Geoffrey Fox and William Goddard has been essential. I thank Paul Messina and Mary Maloney for the convenience provided by Caltech Concurrent Supercomputing Facility. This research is supported in part by the Department of Energy Grant No. (DEGF03-85ER25009).

[1]N. C. Yeh and C. C. Tsuei, Phys. Rev. B **39**, 9708 (1989).

[2]P. C. E. Stamp, L. Forro, and C. Ayache, Phys. Rev. B **38**, 2847 (1988); S. Martin *et al.*, Phys. Rev. Lett. **62**, 677 (1989).

[3]J. M. Kosterlitz and D. J. Thouless, J. Phys. C **6**, 1181 (1973); J. M. Kosterlitz, *ibid.* **7**, 1046 (1974).

[4]T. Matsubara and K. Matsuda, Prog. Theor. Phys. **16**, 569 (1956); **17**, 19 (1957).

[5]D. D. Betts, in *Phase Transition and Critical Phenomena,* edited by C. Domb and M. S. Green (Academic, New York, 1974), Vol. 3, p. 569.

[6]J. Tobochnik and G. V. Chester, Phys. Rev. B **20**, 3761 (1980); R. Gupta *et al.*, Phys. Rev. Lett. **61**, 1996 (1988); U. Wolff, Nucl. Phys. **B322**, 759 (1989).

[7]J. Van Himbergen and S. Chakravarty, Phys. Rev. B **23**, 359 (1981).

[8]J. A. Hertz, Phys. Rev. B **14**, 1165 (1976), M. T. Beal-Monod, Phys. Rev. Lett. **34**, 1465 (1975).

[9](a) J. Rogiers, T. Lookman, D. D. Betts, and C. J. Elliott, Can. J. Phys. **56**, 409 (1978); (b) J. Rogiers, E. W. Grundke, and D. D. Betts, *ibid.* **57**, 1719 (1979).

[10]H. Takano and M. Suzuki, J. Stat. Phys. **26**, 635 (1981), and reference therein.

[11]M. Suzuki, J. Stat. Phys. **43**, 833 (1986); R. M. Fye, Phys. Rev. B **33**, 6271 (1986).

[12]M. Suzuki, S. Miyashita, A. Kuroda, and C. Kawabata, Phys. Lett. **60A**, 478 (1977).

[13]H. De Raedt, B. De Raedt, J. Fivez, and A. Lagendijk, Phys. Lett. **104A**, 430 (1984); H. De Raedt, B. De Raedt, and A. Lagendijk, Z. Phys. B **57**, 209 (1984).

[14]E. Loh, D. J. Scalapino, and P. M. Grant, Phys. Rev. B **31**, 4712 (1985).

[15]Y. Okabe and M. Kikuchi, J. Phys. Soc. Jpn. **57**, 4351 (1988); S. Homma, T. Horiki, H. Matsuda, and N. Ogita (unpublished).

[16]H. Q. Ding and M. S. Makivic, Phys. Rev. Lett. **64**, 1449 (1990); M. S. Makivic and H.-Q. Ding, Phys. Rev. B **43**, 3562 (1991).

[17]G. Fox *et al.*, *Solving Problems on Concurrent Processors* (Prentice-Hall, Englewood, Cliffs, NJ, 1988); H.-Q. Ding, Comput. Phys. Commun. **65**, 92 (1991).

[18]H. Q. Ding and M. S. Makivic, in *Proceedings of the 5th Distributed Memory Computing Conference,* edited by D. Walker and Q. Stroud (IEEE Computer Society, Los Alamitos, 1990).

[19]G. Gemez-Santos and J. D. Joannopoulos, Phys. Rev. B **36**, 8707 (1987).

[20]S. Tang, Phys. Lett. A **129**, 83 (1988); J. Oitmaa and D. D. Betts, Can. J. Phys. **56**, 897 (1978).

[21]H.-Q. Ding and M. S. Makivic, Phys. Rev. B **42**, 6827 (1990).

[22]H.-Q. Ding, J. Phys.: Condens. Matter **2**, 7979 (1990).

[23]J. J. Cullen and D. P. Landau, Phys. Rev. B **27**, 297 (1983).

[24]F. J. Dyson, E. H. Lieb and B. Simon, J. Stat. Phys. **18**, 335 (1978).

[25]K. Binder, *Monte Carlo Methods in Statistical Physics* (Springer-Verlag, Berlin, 1979), p. 1.

[26]L. P. Kadanoff, Physics **2**, 263 (1966).

[27]M. E. Fisher, in *Critical Phenomena,* edited by F. J. W. Hahne, Lecture Notes in Physics, Vol. 186 (Springer-Verlag, New York, 1983).

[28]R. J. Birgeneau, Phys. Rev. B **41**, 2514 (1990).